RSC Advances

PAPER

View Article Online
View Journal | View Issue

Check for updates

Cite this: *RSC Adv.*, 2024, **14**, 14254

Enhanced thermal desorption of chlorinated hydrocarbons by nanoscale zero-valent iron: the effect of *in situ* dechlorination†

Yi Zhu,[a] Xinlei Ren[b] and Minghui Xiang *[b]

Thermal desorption provides an efficient solution to remediate soil contaminated with chlorinated organic pollutants. However, enhanced desorption efficiency is desired to facilitate easier and less costly remediation. Hence, nanoscale zero-valent iron (nZVI) was combined with thermal desorption to remove trichloroethene (TCE) and trichlorobenzene (TCB) from soil in a laboratory-scale study. The addition of nZVI greatly improved the desorption efficiency, especially at low temperature with 99.6% of TCE and 98.8% of TCB removed at 300 °C for 2 h. Characterization results revealed that the addition of nZVI loosened the structure of soil, preventing the soil from agglomerating during the thermal treatment. Besides, the analyses of dechlorination intermediates and the variation of Fe species proved the *in situ* dechlorination effect of nZVI and the redox cycle of Fe was revealed. Moreover, the influences of nZVI dosage and treatment time on thermal treatment were assessed. This study not only offers new perspectives for contaminated soil remediation, but also provides mechanistic insights into the dechlorination effect of nZVI in the thermal desorption.

Received 12th February 2024
Accepted 24th April 2024

DOI: 10.1039/d4ra01077a

rsc.li/rsc-advances

Open Access Article. Published on 30 April 2024. Downloaded on 2/8/2026 2:41:36 AM.
This article is licensed under a Creative Commons Attribution-NonCommercial 3.0 Unported Licence.

Introduction

Chlorinated hydrocarbons (CHs) are a class of synthetic organic chlorinated compounds used in industrial and agricultural activities, most of which exhibit strong carcinogenic, teratogenic, and mutagenic properties. In addition, these molecules are persistent and ubiquitous in the environment, and therefore have received widespread attention worldwide.[1] CHs are widely used as organic solvents and raw materials in paint, pesticides, dry cleaning, chemical industry production, and other fields.[2] The United States Environmental Protection Agency listed CHs as priority control pollutants in the late 1970s. Trichloroethene (TCE) is a typical chlorinated hydrocarbon with low water solubility and strong absorption to soil particles. It is one of the major pollutants in chlorinated hydrocarbons contaminated soil.[3] The Ministry of Ecology and Environment of China has therefore listed TCE a major regulatory priority. In addition, high trichlorobenzene (TCB) concentrations have been detected in the soil and groundwater of China, which will further transfer and accumulate in the environment, and eventually endanger human heath through the food chain.[4–7] Thus, the remediation of CHs-contaminated soil has been a challenge for decades.

To date, methods including chemical oxidation,[8] chemical reduction,[9] steam extraction,[10] thermal desorption,[11] soil washing,[12] bioremediation[13] have been developed to remediate CHs-contaminated soil. Among these methods, thermal desorption was reported to effectively remove volatile, semi-volatile organic matter, and especially chlorinated compounds in contaminated soil.[14] It has attracted increasing attention to remediate contaminated soil due to its advantages of capability to remove different types of pollutants, high efficiency, high safety, short treatment period, and good soil recycling ability.[15] However, the mechanism of thermal desorption is mainly based on physical separation and incineration, which is costly and possibly to generate more toxic substances.[16] The chlorine organic pollutants such as chlorobenzene and polychlorinated biphenyls in the soil have the potential to generate dioxins through precursor synthesis during thermal desorption.[17] Therefore, a technology which thoroughly degrade CHs needs to be developed to lessen secondary contamination of thermal desorption.

Nanoscale zero-valent iron (nZVI) as the most extensively applied nanomaterial for environmental remediation is one of the most promising strategies to effectively remediate halogenated organic compounds.[18–20] For instance, Qu *et al.*[21] developed a P-doped biochar-anchored nZVI material to degrade TCE in groundwater *via* persulfate activation. The different diffusion rate of iron atoms and the shell component triggered multiple Kirkendall effects, which promoted the activation activity of

[a]*Shanghai Chengtou Environmental Ecological Remediation Technology Co., Ltd, Shanghai 200444, PR China*

[b]*Institute of Environmental Pollution and Health, School of Environmental and Chemical Engineering, Shanghai University, Shanghai 200444, PR China. E-mail: Xiangmh@shu.edu.cn*

† Electronic supplementary information (ESI) available. See DOI: https://doi.org/10.1039/d4ra01077a

© 2024 The Author(s). Published by the Royal Society of Chemistry

Open Access Article. Published on 30 April 2024. Downloaded on 2/8/2026 2:41:36 AM. This article is licensed under a Creative Commons Attribution-NonCommercial 3.0 Unported Licence.

persulfate to generate more active species. The strategy effectively promoted the dechlorination and mineralization of TCE. Besides, nZVI-induced chemical reduction is also considered to be effective to dechlorinate TCE into non-toxic products. Dong *et al.*[22] investigated the reduction of TCE by sulfide-modified nZVI. Experimental results indicated that the modified nZVI achieved the complete removal of TCE within 10 h in aqueous solution, indicating the good reduction capability of nZVI. As for the application of nZVI in thermal desorption, Liu *et al.*[23] combined thermal desorption with nZVI to remove polychlorinated biphenyl from soil. The desorption efficiency was greatly improved by nZVI with 98.35% of polychlorinated biphenyl removed in 1 h at 600 °C. However, the influence of nZVI in thermal desorption to remove CHs at low temperature needs to be further investigated. Besides, the detailed mechanism of the enhancement by nZVI is yet ambiguous, which needs to be further elucidated.

Hence, nZVI was applied into thermal desorption to remediate CHs-contaminated soil in which TCE and TCB was the predominant pollutants. The effect of the addition of nZVI on the desorption and *in situ* dechlorination of TCE/TCB at the temperature ranging from 100 to 600 °C was investigated. Characterization methods including X-ray diffraction (XRD), X-ray photoelectron spectroscopy (XPS), and scanning electron microscope (SEM) were utilized to clarify the role of nZVI in thermal desorption and the mechanism of the *in situ* dechlorination. Besides, the effects of temperature, nZVI dosage, and treatment time on thermal desorption were assessed. This study provides mechanistic insights into the dechlorination effect of nZVI in the thermal desorption of CHs, which offers new perspectives for contaminated soil remediation.

Materials and methods

Chemicals

Nanoscale zero-valent iron (nZVI, 98%) and 1,2,4-trichlorobenzene ($C_6H_3Cl_3$, 99%) were purchased from Shanghai Macklin Biochemical Technology Co., Ltd. Trichloroethylene (C_2HCl_3, AR) and ethanol (C_2H_6O, AR) were provided by Sinopharm Chemical Reagent Co., Ltd. Deionised (DI) water was obtained using a Millipore Milli-Q SP Reagent Water System (Milford, MA, USA).

Sample preparation

The contaminated soil used in this study was collected from an industrial site in Shanghai, China. The physicochemical properties of the soil are listed in Table 1. The collected soil sample was firstly air-dried at room temperature and then grinded to pass through a 100-mesh sieve for further thermal desorption.

Table 1 Physicochemical properties of the contaminated soil

Property	Value
pH	8.67
Soil organic matter (g kg^{-1})	10.176
Soil organic carbon (g kg^{-1})	7.003
Soil moisture content (%)	26.9
Cation exchange capacity (cmol+ kg^{-1})	11.989

Thermal desorption performance

Before thermal desorption, nZVI and contaminated soil were mixed uniformly with the dosage of 50 mg g^{-1}. The mixture was then subjected to thermal desorption at different temperatures (100, 200, 300, 400, 500, and 600 °C) for 120 min under nitrogen flow with the heating rate of 10 °C min^{-1} to investigate the effect of temperature (Fig. 1). After the experiment, nZVI was separated with the soil samples by magnet, washed with DI and ethanol and then dried in a vacuum oven at 60 °C overnight. The effect of nZVI dosage on thermal desorption was evaluated by adding different amounts (0, 10, 25, 50, and 100 mg g^{-1}) of nZVI into the contaminated soil and then thermal desorption at 300 °C with the same procedure. Besides, nZVI and contaminated soil were premixed with the dosage of 50 mg g^{-1} and then subjected to thermal desorption at 300 °C for 20, 40, 60 and 120 min to investigate the effect of heating time. All the experiments were conducted in triplicates and the average data with the standard deviations were displayed.

Contaminants analysis

A gas chromatography mass spectrometer (GC-MS, Shimadzu GCMS-QP2020 PLUS) equipped with a MXT-624 (60 m × 0.25 mm × 1.4 μm) column was employed with a flow rate of 1 mL min^{-1} to identify and quantify the contaminants in the soil. The column temperature was originally set at 45 °C and held for 4 min. It was then increased to 150 °C with the heating rate of 8 °C min^{-1}. Subsequently, the temperature was increased to 220 °C with the heating rate of 10 °C min^{-1} and held for 6 min. The solvent delay time was 3.8 min. The temperature of the sample inlet and detector was set at 190 and 220 °C, respectively. An additional sample without thermal treatment was tested in each experimental batch due to the possible evaporation of TCE and TCB during the experimental procedure.

Characterization

XRD patterns of pristine nZVI and those after thermal desorption were obtained from a Rigaku D/max-2200PC X-ray diffractometer with Cu Ka radiation ($\lambda = 1.542$ Å, 40 kV, 40 mA, 1600 W). The elemental compositions of nZVI before and after

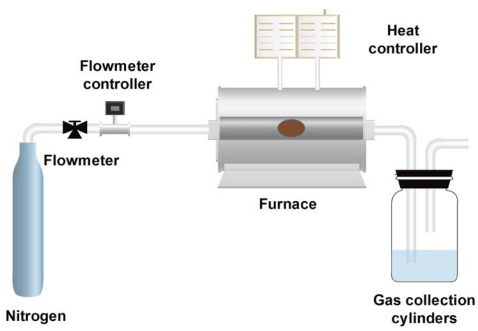

Fig. 1 Scheme of the experimental apparatus.

Open Access Article. Published on 30 April 2024. Downloaded on 2/8/2026 2:41:36 AM. This article is licensed under a Creative Commons Attribution-NonCommercial 3.0 Unported Licence.

reaction was determined by XPS using a Thermo Scientific K-Alpha X spectrometer. The original binding energy was normalized to the C 1s peak at 284.8 eV. The morphology and structure of the samples was observed using a scanning electron microscopy (ZEISS Gemini SEM 300) equipped with energy dispersive X-ray spectrometer (EDS). The magnetic properties of nZVI were monitored using a vibrating sample magnetometer (VSM, MPMS XL-7).

Results and discussions

Characterization of nZVI and soil samples

The crystalline structure of the nZVI used in this study was analysed by XRD. As shown in Fig. 2a, the characteristic diffraction peaks at 44.9°, 65.0°, and 82.3° were attributed to (110), (200), and (211) facets of Fe,[24,25] indicating the good crystalline structure of commercial nZVI. Furthermore, the surface elemental composition of the pristine nZVI were provided by XPS. The Fe 2p high-resolution spectrum of the pristine nZVI was illustrated in Fig. 2b. The peaks located at 707.2, 710.6, 712.4 eV were attributed to the Fe $2p_{3/2}$ of Fe^0, Fe^{2+}, and Fe^{3+}, respectively.[26–28] Besides, the peaks at 724.1 and 725.9 eV were assigned to the Fe $2p_{1/2}$ of Fe^{2+} and Fe^{3+} respectively while those at 714.7, 719.2, 727.7, and 733.7 eV corresponded to the satellite peaks.[29,30] The fraction of the Fe species was calculated to be 2.0% (Fe^0), 58.8% (Fe^{2+}), and 39.2% (Fe^{3+}). The magnetic property of the nZVI was further investigated by the VSM. Fig. 2c showed a ferromagnetic-type curve with hysteresis loops, indicating the great magnetic properties of nZVI.[30] Therefore, nZVI could easily be separated from the soil after thermal desorption, which made it easier to recycle and reuse, reducing the possible secondary pollution to the environment.

The morphology of the pristine nZVI and the contaminated soil was monitored by SEM. The pristine nZVI showed a spherical shape with a particle size of about 200 nm (Fig. 3a). The structure of raw soil without treatment exhibited a dense irregular shape (Fig. 3b–d). After the addition of nZVI, the soil particle structure became loose and the morphology changed from particles with irregular shapes to lamellar structure (Fig. 3e and f). Compared with the particle structure of raw soil, the looser lamellar structure is more favourable for the desorption of TCE and TCB. After thermal desorption of nZVI-added soil at 300 °C for 2 h, the SEM images of soil particles were shown in Fig. 3g and h. It can be seen that the structure of nZVI-added soil after thermal desorption changed considerably with the structure becoming denser and the reduction of the number of pores. Moreover, an irregular particle morphology of the soil was presented, which was similar to the structural characteristics of raw soil before thermal desorption. The change in the morphology of the soil might be attributed to the sintering agglomeration of the soil at high temperature.

In order to further investigate the effect of added nZVI on the morphological changes of the soil and its role in thermal desorption, we analyzed the elemental distributions of the three soils mentioned above (raw soil, nZVI-added soil before thermal desorption and after thermal desorption) by EDS. As shown in Fig. 3i, C, O, Fe and Cl elements are uniformly distributed in raw soil, indicating that TCE/TCB and Fe existed in the raw soil homogeneously. However, a large increase in the content of Fe elements was witnessed in nZVI-added soil and its distribution exhibited a regional pattern, suggesting that nZVI was successfully added into the soil (Fig. 3j). It is worth noting that C, O and Cl remained uniformly distributed in nZVI-added soil, which indicated that simply adding nZVI into the soil did not exhibit a significant effect on the elemental composition and distribution in the soil. Interestingly, agglomeration of Fe elements occurred in the nZVI-added soil after thermal desorption (Fig. 3k). It was reported that nZVI tends to aggregate when reacting in aqueous solution and subsequently agglomerates into large particles.[21,30] The transformation of the soil from loose flaky structure to dense irregular particles after thermal desorption in the previous analyses might be attributed to the agglomeration of nZVI. In addition to Fe, C and Cl also showed agglomeration phenomenon with the agglomeration area in consistent with that of Fe. This phenomenon suggested that the organic matter (including TCE and TCB) in the contaminated soil might aggregate on the surface of nZVI and underwent chemical reactions during the thermal desorption process.

nZVI enhanced thermal desorption of TCE/TCB from the soil

The residual concentration of TCE/TCB in various soil samples was measured to investigate of effect of nZVI addition on thermal desorption at different temperatures (100, 200, 300,

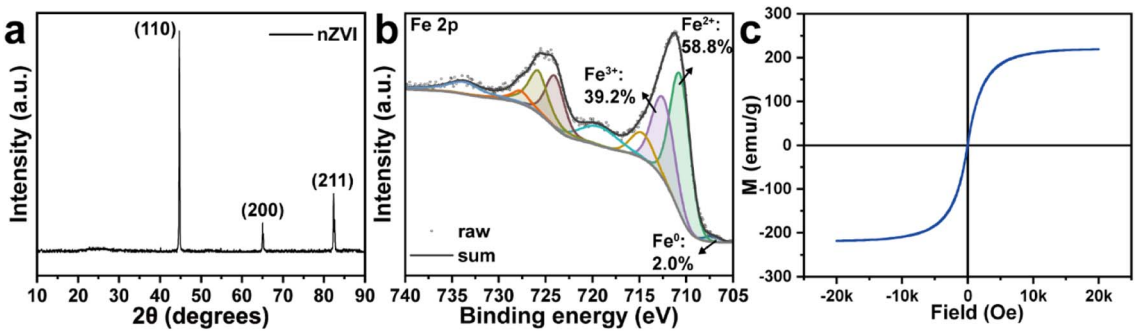

Fig. 2 (a) XRD pattern, (b) XPS spectrum, and (c) magnetic hysteresis loops of pristine nZVI.

© 2024 The Author(s). Published by the Royal Society of Chemistry

Open Access Article. Published on 30 April 2024. Downloaded on 2/8/2026 2:41:36 AM.
This article is licensed under a Creative Commons Attribution-NonCommercial 3.0 Unported Licence.

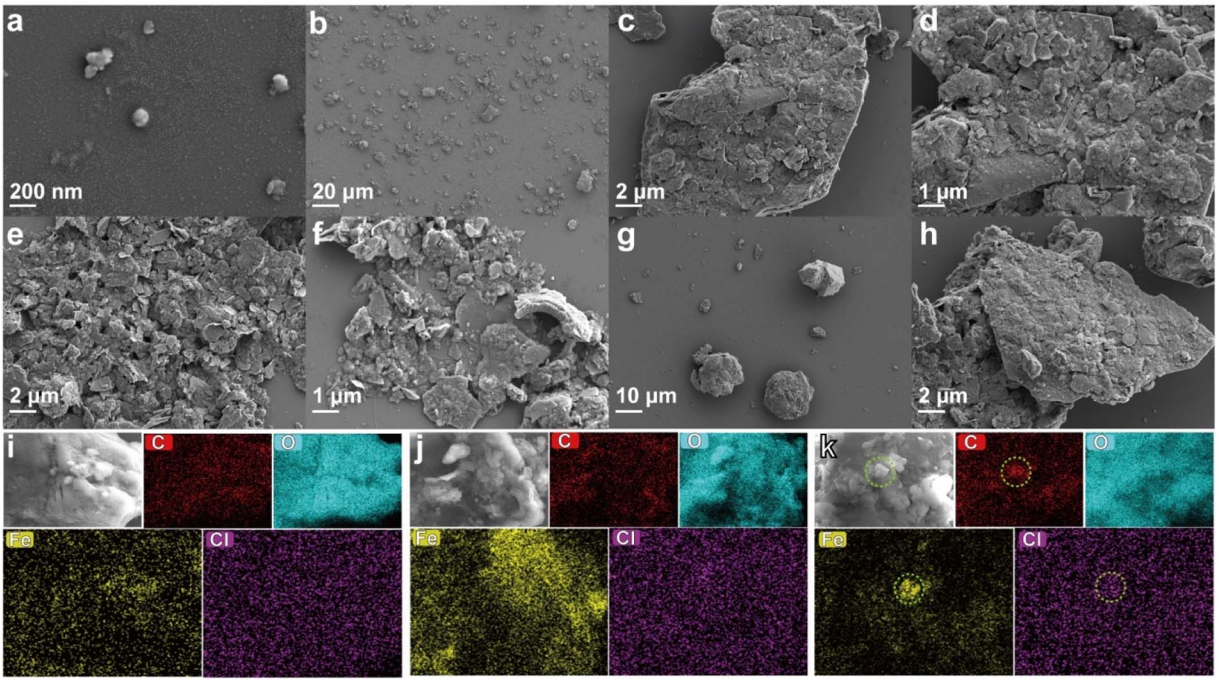

Fig. 3 SEM images of (a) pristine nZVI, (b)–(d) raw soil, (e) and (f) soil with the addition of nZVI, (g) and (h) soil after thermal desorption with the addition of nZVI, the EDS mapping images of (i) raw soil, (j) soil with the addition of nZVI, and (k) soil after thermal desorption with the addition of nZVI.

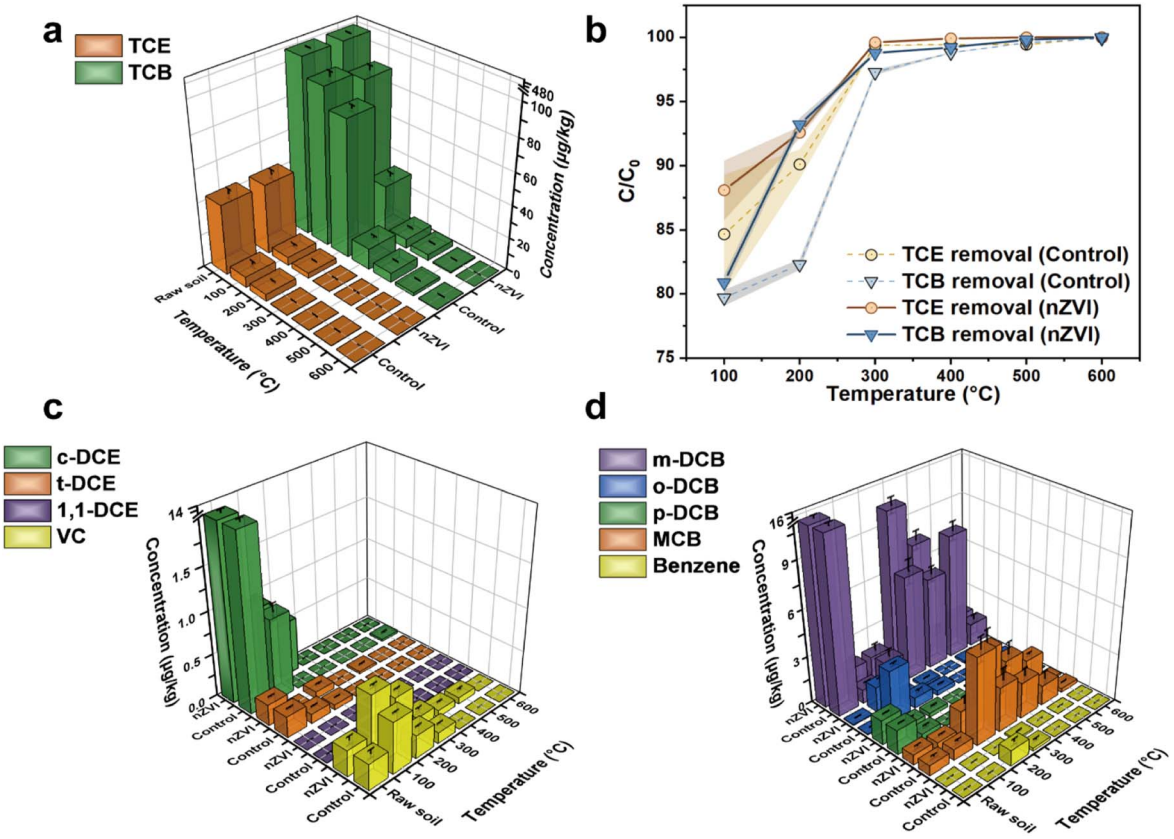

Fig. 4 (a) Concentration of TCE and TCB in different soil samples, (b) removal efficiency of TCE and TCB at different temperatures, dechlorination intermediates of (c) TCE and (d) TCB.

Open Access Article. Published on 30 April 2024. Downloaded on 2/8/2026 2:41:36 AM. This article is licensed under a Creative Commons Attribution-NonCommercial 3.0 Unported Licence.

400, 500, and 600 °C). The efficiency was evaluated by comparing the residual concentration of TCE/TCB with the initial concentration in raw soil. As shown in Fig. 4a, the concentration of TCE and TCB in raw soil without any treatment was 43.28 and 478.91 μg kg^{-1}, respectively. After thermal treatment in the absence of nZVI at 100 °C for 2 h, the concentration decreased to 6.63 (TCE) and 97.24 (TCB) μg kg^{-1} with the removal efficiency of 84.67 and 79.69%, respectively (Fig. 4b). With the addition of nZVI the concentration of TCE and TCB subsequently decreased to 5.16 and 91.57 μg kg^{-1} respectively. The removal efficiency was slightly enhanced by the addition of nZVI with the improvement of 3.41% for TCE and 1.19% for TCB, indicating that the limited enhancement of nZVI at low temperature (100 °C). However, thermal desorption efficiency of TCB was substantially promoted (93.21% compared with 80.88% at 100 °C) with the heating temperature further increased to 200 °C. Even in comparison with the control group, the addition of nZVI greatly improved the removal of TCB with the increasement of 10.92% in efficiency. Besides, the increase in temperature effectively promoted the desorption of TCE as well. Although nZVI still exhibited superior efficiency, the efficiency exceeded 90% with or without nZVI. When the heating temperature further increased (≥300 °C), the efficiency difference between control group and nZVI group decreased. For instance, the TCE removal efficiency of control group and nZVI group was 99.37% and 99.60%, respectively. Similarly, the desorption efficiency of TCB were 97.27% (control) and 98.78% (nZVI). As the treatment temperature reached 600 °C, 100% of TCE evaporated from the soil while for TCB 100% removal efficiency was achieved in nZVI group and only 99.92% was desorbed in control group. Overall, the results indicated that the addition of nZVI effectively enhanced the desorption of TCE/TCB by thermal desorption, especially when the process was conducted at low temperature.

According to previous literatures,[31,32] TCE could be dechlorinated to vinyl chloride (VC), *trans*-1,2-dichloroethylene (*t*-DCE), *cis*-1,2-dichloroethylene (*c*-DCE), and 1,1-dichloroethylene (1,1-DCE) while TCB could be dechlorinated to 1,2-dichlorobenzene (*o*-MCB), 1,4-dichlorobenzene (*p*-MCB), 1,3-dichlorobenzene (*m*-DCB), chlorobenzene (MCB), and benzene. Thus, the dechlorination intermediates were identified to further investigate the role of nZVI in thermal desorption (Fig. 4c and d). Since that the raw soil were collected from an actual polluted site, some of the dechlorination intermediates were detected without treatment. As shown in Fig. 4c, 1,1-DCE was not detected in all the soil samples, indicating that it was not generated during the thermal desorption process. The concentration of *c*-DCE decreased from 12.12 μg kg^{-1} in raw soil to 0.96 (control) and 0.95 (nZVI) μg kg^{-1} after thermal desorption at 100 °C, which was mainly due to the desorption of *c*-DCE. Furthermore, *c*-DCE was barely detected in control group when the heating temperature was over 200 °C. However, 0.62 μg kg^{-1} of *c*-DCE was still detected in nZVI group after thermal treatment at 200 °C. Given that the TCE desorption efficiency was substantially enhanced by the addition of nZVI, the *c*-DCE could be generated by the dechlorination of TCE by nZVI during thermal treatment. Interestingly, the concentration of VC in nZVI group was lower than that in control group at all the temperatures, indicating that nZVI effectively promoted the desorption and dechlorination of VC. Similarly, the concentration of TCB dechlorination intermediates exhibited volcano-like curves as the temperature increased, indicating the accumulation of intermediates during the adsorption of TCE and TCB. Besides, the nZVI group generated more intermediates (especially *m*-DCB and MCB) compared with control group, which further confirmed the dechlorination of TCB by nZVI. The particle size distribution of the soil was further analyzed to investigate the effect of thermal desorption and the addition of nZVI on soil texture properties. As shown in Fig. S1,† the particle size gradually became larger with the increase of the thermal desorption temperature, indicating that the soil might agglomerate during the process. When the temperature was 300 °C or below, the addition of nZVI exhibited little effect on soil particle size. However, the particle size of the soil after thermal desorption with nZVI addition was significantly smaller than that of the control group as the temperature was increased over 300 °C. The result was consistent with the SEM results, indicating that the addition of nZVI effectively inhibited the agglomeration of the soil at high temperatures. Besides, nZVI also exhibited superior efficiency on thermal desorption of other CHs in the soil, which facilitates its application for actual environmental remediation (Fig. S2†).

Effect of nZVI dosage on thermal desorption

The influence of nZVI dosage on TCE/TCB removal was investigated by adding different amounts (10, 25, 50, and 100 mg g^{-1}) of nZVI into the contaminated soil and subsequently thermal desorption at 300 °C for 2 h. With the increase of nZVI addition, the residual concentration of TCE in the soil only slightly changed from 0.274 μg kg^{-1} at the dosage of 0 mg g^{-1} to 0.173 μg kg^{-1} at the dosage of 50 mg g^{-1} (Fig. 5a). The TCE in the soil was completely removed as the nZVI dosage was further increased to 100 mg g^{-1}. As shown in Fig. 5b, almost negligible increasement was witnessed in the removal efficiency of TCE as more nZVI were added. The results indicated that nZVI demonstrated no obvious efficiency in the thermal desorption of trace TCE while the removal of TCE might depend on the treatment temperature.[33] On the contrary, the removal of TCB was positively correlated with the dosage of nZVI. With the increase of the dosage, the concentration of residual TCB in the soil decreased from 13.072 μg kg^{-1} (0 mg g^{-1}) to 1.579 μg kg^{-1} (100 mg g^{-1}), and the removal rate of TCB increased from 72.9% to 96.4%, indicating that nZVI effectively promoted the thermal desorption of TCB (Fig. 5a and b). Moreover, the dechlorination intermediates with different nZVI dosages were analyzed. Only a small amount of VC (≤0.157 μg kg^{-1}) after the thermal desorption of TCE whether with or without nZVI, further confirming that the removal of TCE was more reliable on temperature (Fig. 5c). The concentration of intermediate MCB showed a gradual increase as more nZVI was added, indicating that the increase of nZVI dosage promoted the dechlorination of TCB (Fig. 5d). Furthermore, the particle size of the soil after thermal desorption was investigated. The dosage of nZVI exhibited little impact of the particle size distribution of the soil, demonstrating that nZVI was an environmental-friendly additive (Fig. S3†).

© 2024 The Author(s). Published by the Royal Society of Chemistry

Open Access Article. Published on 30 April 2024. Downloaded on 2/8/2026 2:41:36 AM.
This article is licensed under a Creative Commons Attribution-NonCommercial 3.0 Unported Licence.

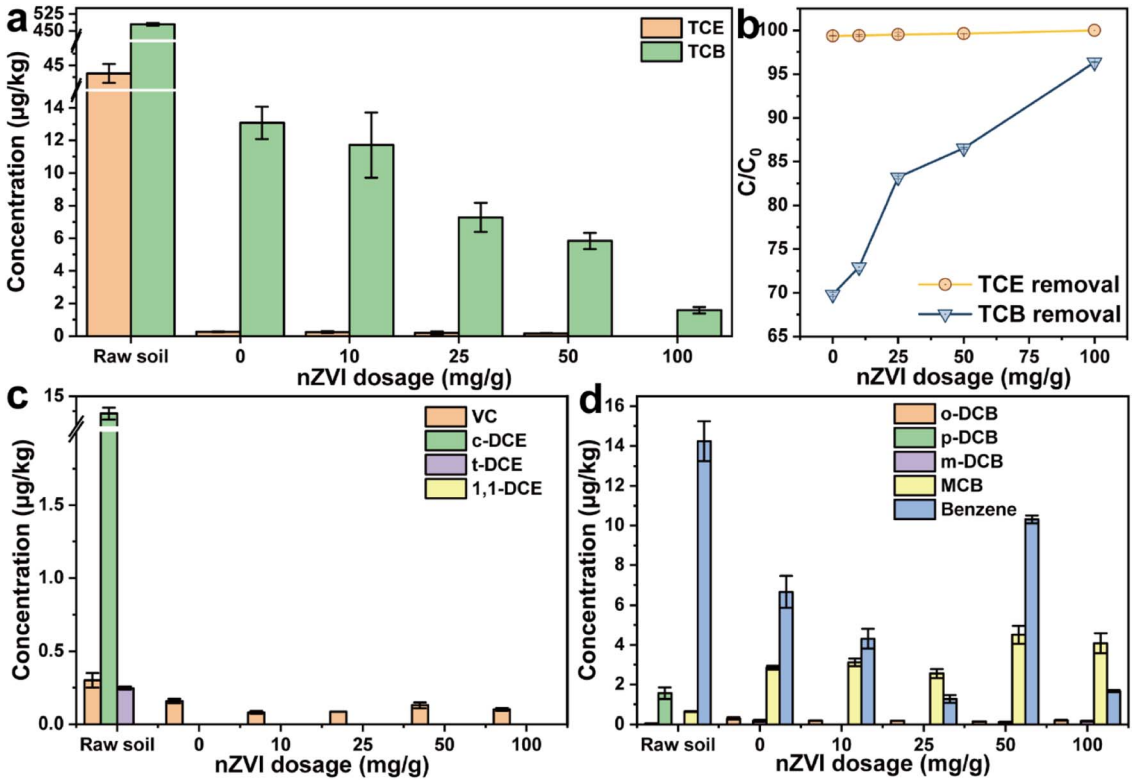

Fig. 5 (a) Concentration of TCE and TCB in different soil samples, (b) removal efficiency of TCE and TCB, dechlorination intermediates of (c) TCE and (d) TCB with different nZVI dosages.

Effect of treatment time on thermal desorption

The impact of the treatment time on TCE/TCB removal was investigated by adding 50 mg g^{-1} nZVI into the contaminated soil and thermal desorption at 300 °C for different time (20, 40, 60, and 120 min). Interestingly, experimental results showed that the residual concentrations of TCE and TCB in the soil did not decrease significantly with the increase of thermal desorption time (Fig. 6a). The removal efficiency only slightly increased with the increase of thermal desorption time, indicating that the decisive factor determining the final efficiency of thermal desorption might not be the treatment time to remove CHs. As depicted in Fig. 6c, a large amount of TCE dechlorination product (*t*-DCE) were generated at the treatment time of 20 min, which confirmed the dechlorination effect of nZVI on TCE. With the further increase of treatment time, the intermediate product *t*-DCE was also removed from the soil. The main dechlorination products of TCB (MCB and benzene) also showed an increasing trend with the increase of desorption time, indicating the dechlorination effect of nZVI on TCB during the thermal desorption process (Fig. 6d). In addition, the treatment time had no significant effect on the particle size distribution of the soil, demonstrating that the agglomeration of the soil was mainly related to the thermal desorption temperature (Fig. S4†).

Mechanism of *in situ* dechlorination

The XRD patterns of nZVI after thermal desorption was further obtained to investigate the changes of crystalline structure during the reaction. As shown in Fig. 7, the crystal structure of nZVI after thermal desorption at 100, 200, and 300 °C was almost consistent with the pristine nZVI. When the thermal desorption temperature was further increased to 400 °C, a new peak was observed in the XRD pattern at $2\theta = 35.3°$, which belonged to the characteristic diffraction peak of Fe_3O_4, indicating that part of nZVI was oxidized into Fe_3O_4 in the process of high-temperature thermal desorption. Furthermore, the peak at 35.3° became sharper and the new diffraction peaks at 30.2°, 43.2°, 57.2° and 62.8° were also attributed to Fe_3O_4 as the temperature was further increased to 500 °C and 600 °C, which might be due to the oxidation of nZVI with soil organic matter (SOM) in the soil. In addition, when the temperature was further increased to 500 °C and 600 °C, the characteristic diffraction peaks belonging to SiO_2 were observed at 21.0°, 26.7°50.2°, 60.0° and 68.2° in the XRD patterns of nZVI, indicating that minerals in the soil agglomerated on the surface of nZVI at high temperatures, verifying the interaction between nZVI and soil in thermal desorption. The changes in element composition and valence of nZVI were analyzed to investigate the mechanism in thermal desorption and dechlorination to remove TCE and TCB.[34] As illustrated in Fig. 8a–c, Fe^0 still existed in nZVI at very low percentages after thermal desorption at 100, 200 and 300 °C, which confirmed the characterization results of XRD, indicating that the element composition and distribution of nZVI did not change significantly in the process of low-temperature thermal desorption. Meanwhile, characterization results revealed that as the increase of thermal desorption temperature from 100 °C to

Open Access Article. Published on 30 April 2024. Downloaded on 2/8/2026 2:41:36 AM.
This article is licensed under a Creative Commons Attribution-NonCommercial 3.0 Unported Licence.

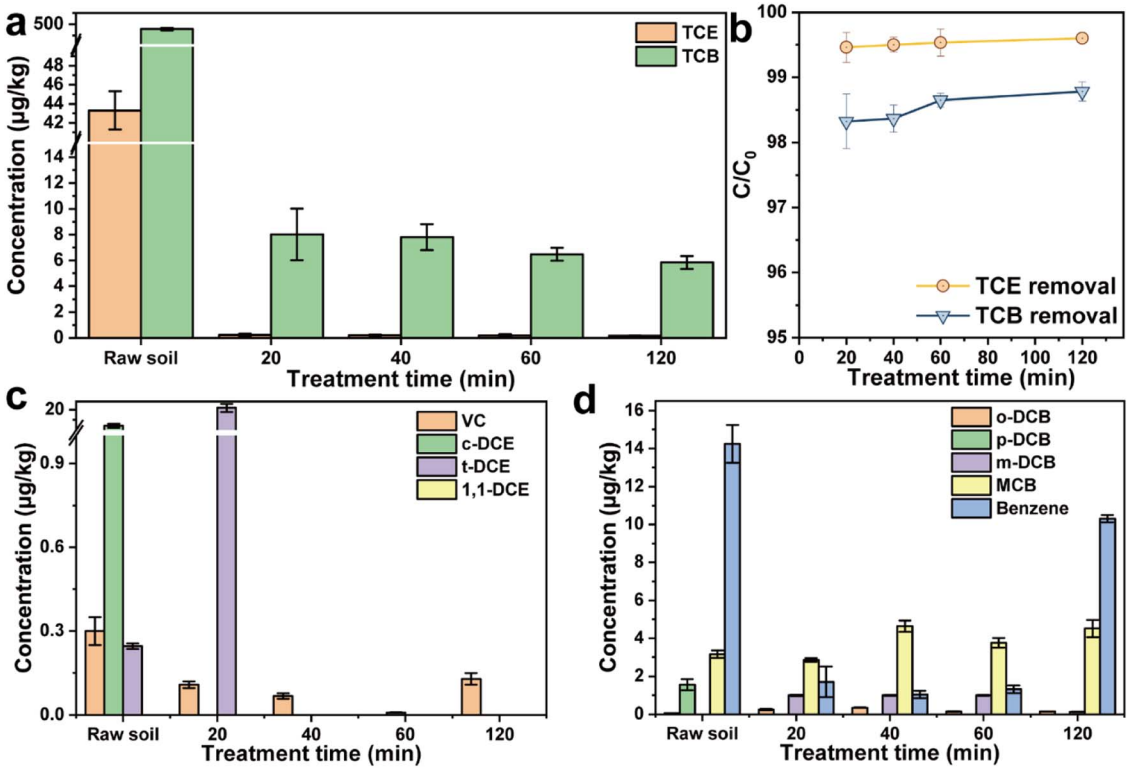

Fig. 6 (a) Concentration of TCE and TCB in different soil samples, (b) removal efficiency of TCE and TCB, dechlorination intermediates of (c) TCE and (d) TCB with different treatment times.

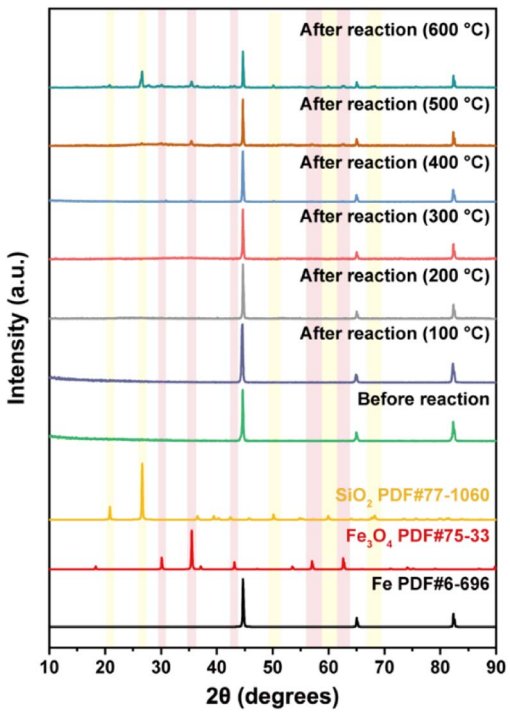

Fig. 7 XRD patterns of nZVI before and after thermal desorption at different temperatures.

300 °C, the distribution of Fe^0 and Fe^{2+} increased, while the content of Fe^{3+} gradually decreased. This might be attributed to that the oxidized Fe species in the oxidation layer on the surface of nZVI reacted with the SOM in the soil at high temperature. Through carbothermal reduction, the SOM reduced the oxidized Fe species to Fe^0, while the SOM was transformed into carbon.[26] Interestingly, it was concluded from Fig. 4 that the presence of nZVI did promote the thermal desorption and reduction dechlorination of TCE and TCB. This indicated that a potential redox cycle of Fe species existed in the thermal desorption process. Firstly, Fe^0 reduced TCE and TCB to form intermediates and was subsequently oxidized to Fe^{2+} and Fe^{3+} (eqn (1)–(3)). Afterwards, the SOM reduced Fe^{3+} to Fe^{2+}/Fe^0 and further reduced Fe^{2+} to Fe^0 at high temperature (eqn (4)–(6)). When the thermal desorption temperature reaches 400 and 500 °C, the existence of Fe^0 was not in the XPS spectrum after the reaction, indicating that all Fe^0 species were involved in the reduction process and oxidized to Fe^{2+} and Fe^{3+} (Fig. 8d and e). The results demonstrated that the rate of Fe^0 contributing to the reduction of TCE/TCB was higher than that of carbothermal reduction at high desorption temperature, ultimately leading to the decrease of Fe^0/Fe^{2+} content. During this process, the removal efficiency of TCE/TCB almost reached 100% and a large number of intermediates were generated. When the temperature reached 600 °C, the concentration of pollutants in the soil was at a very low level and the carbothermal reduction process dominated. Therefore, Fe^{3+} were reduced to Fe^{2+}, resulting in the increase of Fe^{2+} composition (Fig. 8f).

© 2024 The Author(s). Published by the Royal Society of Chemistry

Open Access Article. Published on 30 April 2024. Downloaded on 2/8/2026 2:41:36 AM.
This article is licensed under a Creative Commons Attribution-NonCommercial 3.0 Unported Licence.

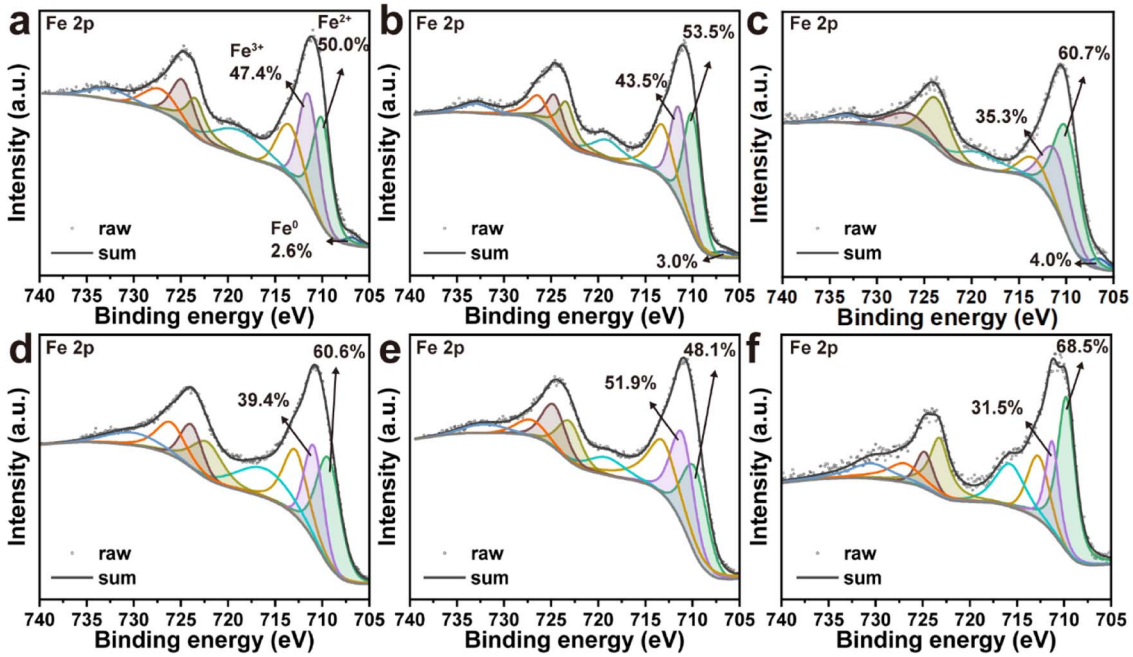

Fig. 8 XPS spectra nZVI after thermal desorption at (a) 100 °C, (b) 200 °C, (c) 300 °C, (d) 400 °C, (e) 500 °C, and (f) 600 °C.

$$Fe^0 + TCE/TCB \rightarrow Fe^{2+} + intermediates \quad (1)$$

$$Fe^0 + TCE/TCB \rightarrow Fe^{3+} + intermediates \quad (2)$$

$$Fe^{2+} + TCE/TCB \rightarrow Fe^{3+} + intermediates \quad (3)$$

$$SOM + Fe^{3+} \rightarrow Fe^{2+} + C \quad (4)$$

$$SOM + Fe^{3+} \rightarrow Fe^0 + C \quad (5)$$

$$SOM + Fe^{2+} \rightarrow Fe^0 + C \quad (6)$$

Conclusions

In this study, nZVI was added into the CHs-contaminated soil as additive to enhance thermal desorption to remove TCE and TCB. Experimental results indicated that the addition of nZVI greatly improved the desorption efficiency at low temperature with 99.6% (TCE) and 98.8% (TCB) removed at 300 °C for 2 h. SEM, laser particle size analyser, and XPS analyses revealed that the addition of nZVI loosened the structure of soil, which prevented it from agglomerating during the thermal treatment. Besides, the detection of dechlorination intermediates and the changes in Fe species proved the *in situ* dechlorination effect of nZVI and the redox cycle of Fe was investigated. Moreover, the effect of nZVI dosage and treatment time on thermal treatment were assessed. This study not only provides mechanistic insights into the dechlorination effect of nZVI in the thermal desorption, but also offers new perspectives for contaminated soil remediation.

Author contributions

Yi Zhu: supervision, writing – review & editing, project administration, funding acquisition. Xinlei Ren: conceptualization, methodology, investigation, writing – original draft, visualization. Minghui Xiang: conceptualization, supervision, writing – review & editing, project administration, funding acquisition.

Conflicts of interest

There are no conflicts of interest to declare.

Acknowledgements

This work was supported jointly by the Shanghai Municipal State-owned Assets Supervision and Administration Commission Enterprise Technology Innovation and Capability Enhancement Project – R&D and Engineering Demonstration of Key Technology for Intelligent Solid Waste Environmental Logistics and Harmless Disposal Based on 5 G+AI (2021011), National Natural Science Foundation of China (42277021) and the National Science Fund for Distinguished Young Scholars (42125706). We would also like to thank Shiyanjia Lab (**https://www.shiyanjia.com**) and the anonymous referees for their helpful comments on this paper.

Notes and references

1 Z. Gong, X. Wang, Y. Tu, J. Wu, Y. Sun and P. Li, *Chemosphere*, 2010, **79**, 138–143.
2 Y. S. Cho, J.-C. Park, B.-S. Choi, J. Moon and J. Yi, in *Studies in Surface Science and Catalysis*, ed. G. F. Froment and K. C. Waugh, Elsevier, 2001, vol. 133, pp. 559–564.

Open Access Article. Published on 30 April 2024. Downloaded on 2/8/2026 2:41:36 AM. This article is licensed under a Creative Commons Attribution-NonCommercial 3.0 Unported Licence.

3 D. M. Hamby, *Sci. Total Environ.*, 1996, **191**, 203–224.
4 H. Zhang, Y. Wang, C. Sun, M. Yu, Y. Gao, T. Wang, J. Liu and G. Jiang, *Environ. Sci. Technol.*, 2014, **48**, 1525–1531.
5 Y. Yuan, X.-a. Ning, Y. Zhang, X. Lai, D. Li, Z. He and X. Chen, *Ecotoxicology*, 2020, **193**, 110257.
6 J. Zhang, C. Li, S. Yin, Y. Wang, Y. Zhou, S. Wang, X. Xu, W. Liu and L. Xu, *Sci. Total Environ.*, 2021, **767**, 145153.
7 J. Zhang, W. Zhao, J. Pan, L. Qiu and Y. Zhu, *Environ. Int.*, 2005, **31**, 855–860.
8 C. Liang, C. J. Bruell, M. C. Marley and K. L. Sperry, *Chemosphere*, 2004, **55**, 1213–1223.
9 P. J. Dorathi and P. Kandasamy, *J. Environ. Sci.*, 2012, **24**, 765–773.
10 J. T. Albergaria, M. d. C. M. Alvim-Ferraz and C. Delerue-Matos, *Chemosphere*, 2008, **73**, 1557–1561.
11 K. Yu, X. Yang, M. Wan, H. Jiang, P. Shao, L. Yang, H. Shi and X. Luo, *J. Hazard. Mater.*, 2023, **442**, 130019.
12 L. V. Pavel and M. Gavrilescu, *Environ. Eng. Manage. J.*, 2008, **7**, 815–834.
13 Z. Xiao, W. Jiang, D. Chen and Y. Xu, *Ecotoxicology*, 2020, **202**, 110925.
14 L. Zhao, H. Hou, K. Shimoda, A. Terada and M. Hosomi, *Chemosphere*, 2012, **88**, 1368–1374.
15 C. Zhao, Y. Dong, Y. Feng, Y. Li and Y. Dong, *Chemosphere*, 2019, **221**, 841–855.
16 Z. Yun, F. Fan, Z. Wu, M. Yin, L. Zhao, Z. Huang and H. Hou, *Chemosphere*, 2022, **286**, 131925.
17 Z. Qi, T. Chen, S. Bai, M. Yan, S. Lu, A. Buekens, J. Yan, C. Bulmău and X. Li, *Environ. Sci. Pollut. Res.*, 2014, **21**, 4697–4704.
18 A. N. Garcia, Y. Zhang, S. Ghoshal, F. He and D. M. O'Carroll, *Environ. Sci. Technol.*, 2021, **55**, 8464–8483.
19 C. Ling, S. Wu, J. Han, T. Dong, C. Zhu, X. Li, L. Xu, Y. Zhang, M. Zhou and Y. Pan, *Water Res.*, 2022, **220**, 118676.
20 F. Gao, M. Zhang, X. Yang, S. Ahmad and J. Tang, *Chem. Eng. J.*, 2023, **461**, 141953.
21 J. Qu, Z. Li, F. Bi, X. Zhang, B. Zhang, K. Li, S. Wang, M. Sun, J. Ma and Y. Zhang, *Proc. Natl. Acad. Sci. U. S. A.*, 2023, **120**, e2304552120.
22 H. Dong, C. Zhang, J. Deng, Z. Jiang, L. Zhang, Y. Cheng, K. Hou, L. Tang and G. Zeng, *Water Res.*, 2018, **135**, 1–10.
23 J. Liu, T. Chen, Z. Qi, J. Yan, A. Buekens and X. Li, *Environ. Sci. Pollut. Res.*, 2014, **21**, 12739–12746.
24 J. Zhang, C. Wang, M. Xiang, Y. Huang, L. Jin, Z. Yang and H. Li, *Chem. Eng. J.*, 2022, **428**, 131779.
25 F. Gao, H. Lyu, S. Ahmad, S. Xu and J. Tang, *Appl. Catal., B*, 2023, **324**, 122246.
26 H. Li, X. Ren, W. Pan, S. Zhu, J. Zhang, Z. Yang, L. Qian, Y. Wang, Y. Huang, L. Guo and M. Xiang, *J. Environ. Chem. Eng.*, 2024, **12**, 112062.
27 J. Zhang, C. Wang, N. Huang, M. Xiang, L. Jin, Z. Yang, S. Li, Z. Lu, C. Shi, B. Cheng, H. Xie and H. Li, *J. Hazard. Mater.*, 2022, **434**, 128913.
28 S. Chen, X. Li, C. W. Kao, T. Luo, K. Chen, J. Fu, C. Ma, H. Li, M. Li, T. S. Chan and M. Liu, *Angew Chem. Int. Ed. Engl.*, 2022, **61**, e202206233.
29 S. Wang, L. Xu and J. Wang, *Environ. Sci. Technol.*, 2021, **55**, 15412–15422.
30 M. Xiang, M. Huang, H. Li, W. Wang, Y. Huang, Z. Lu, C. Wang, R. Si and W. Cao, *Chem. Eng. J.*, 2021, **417**, 129208.
31 Z. Xing, S. Chen, F. Xu, X. Su, F. Gou, Y. Shi, H. Chen, J. Xiang, J. Li and T. Zhao, *J. Environ. Manage.*, 2023, **344**, 118509.
32 J. Wang, J. Xiong, Q. Feng, Z. Wan, Z. Zhou, B. Xiao, J. Zhang and O. Singdala, *J. Environ. Manage.*, 2022, **318**, 115595.
33 C. Bulmău, C. Mărculescu, S. Lu and Z. Qi, *J. Geochem. Explor.*, 2014, **147**, 298–305.
34 N. Li, R. Li, X. Duan, B. Yan, W. Liu, Z. Cheng, G. Chen, L. Hou and S. Wang, *Environ. Sci. Technol.*, 2021, **55**, 16163–16174.

© 2024 The Author(s). Published by the Royal Society of Chemistry